Measurement of rotational dynamics by the simultaneous nonlinear analysis of optical and EPR data

Eric J. Hustedt, Charles E. Cobb, Albert H. Beth, and Joseph M. Beechem
Molecular Physiology and Biophysics, Vanderbilt University, Nashville, Tennessee 37232

ABSTRACT In the preceding companion article in this issue, an optical dye and a nitroxide radical were combined in a new dual function probe, 5-SLE. In this report, it is demonstrated that time-resolved optical anisotropy and electron paramagnetic resonance (EPR) data can be combined in a single analysis to measure rotational dynamics. Rigid-limit and rotational diffusion models for simulating nitroxide EPR data have been incorporated into a general non-linear least-squares procedure based on the Marquardt-Levenberg algorithm. Simultaneous fits to simulated time-resolved fluorescence anisoptropy and linear EPR data, together with simultaneous fits to experimental time-resolved phosphorescence anisotropy decays and saturation transfer EPR (ST-EPR) spectra of 5-SLE noncovalently bound to bovine serum albumin (BSA) have been performed. These results demonstrate that data from optical and EPR experiments can be combined and globally fit to a single dynamic model.

INTRODUCTION

Time-resolved optical anisotropy and electron paramagnetic resonance (EPR) have both been used extensively to measure the rotational dynamics of biological molecules. In the preceeding companion article (1), a new dual function probe, 5-SLE, for the study of rotational dynamics of biomolecules was introduced. We focus here on the development of methods for the analysis of data obtained using this new probe, or any combination of optical and EPR probes. We have incorporated models for simulating nitroxide EPR spectra into a general nonlinear least-squares analysis program, based on the Marquardt-Levenberg algorithm, which has been widely applied to the analysis of optical experiments (2, 3). This approach has proven useful for the analysis of EPR data alone. More importantly, as we focus on here, data from both optical and EPR experiments can be simultaneously fit with a common set of motional parameters.

Time-resolved optical anisotropy, both fluorescence and phosphorescence, have been widely used to measure rotational correlation times (4). The techniques are complementary in that fluorescence is sensitive to motions whose correlation times are in the range of $10^{-11} < \tau_r < 10^{-6}$ seconds with appropriate fluorophores, while phosphorescence is sensitive to motions in the range $10^{-6} < \tau_r < 10^{0}$ seconds. Transient absorption anisotropy (5) and fluorescence recovery (6) are two additional methods that bridge the sensitivity ranges of the fluorescence and phosphorescence emission anisotropy methods. The use of EPR with nitroxide spin-labels to study the dynamics of lipids, DNA, proteins, and membrane bound proteins has been extensively reviewed (7, 8, 9, 10). Conventional linear EPR spectra of nitroxide spin-labels are sensitive to motions whose correlation times are in the range $10^{-11} < \tau_r < 10^{-6}$ seconds (11). The complementary saturation transfer EPR (ST-EPR) technique is sensitive to motions in the range $10^{-6} < \tau_r < 10^{-3}$ seconds (12, 13). Thomas has compared the experimental and theoretical aspects of time-resolved phosphorescence anisotropy and ST-EPR (14, 15).

Few attempts have been made to simultaneously analyze optical and EPR data. Recently, Burghardt and coworkers (16, 17) simultaneously analyzed, using linear least-squares, steady-state fluorescence and linear EPR data from a combination of different probes to find a consistent model for the orientational distributions of myosin cross-bridges under two physiologically relevant conditions. This work demonstrated the advantage of combining EPR and optical data for mapping angular transitions of contractile proteins or other ordered systems.

Nonlinear analysis of multiple data sets, an approach commonly called global analysis, has proven to be a very important technique for analyzing data from various optical techniques (18). This method is ideally suited for the analysis of data from the dual probe, 5-SLE, or from data obtained using separate spin-label and optical probes. The only requirement is that a mathematical relationship exists between the parameters used to model the two data types. In the case of optical anisotropy and EPR, the rotational diffusion coefficients can be directly linked. Conveniently, time-resolved fluorescence anisotropy and linear EPR are sensitive to motions on the same time scale. The same is true of time-resolved phosphorescence anisotropy and ST-EPR.

Computational methods for the simulation of the EPR spectrum of a nitroxide spin-label undergoing rotational diffusion have been developed by McConnell and co-workers (11, 13), Freed and co-workers (19) and Robinson and Dalton (20). In general, however, only a very limited number of attempts at developing rigorous statistical methods for the analysis of nitroxide EPR data have been made. Fajer et al. (21) have developed a program for fitting nitroxide powder patterns (rigid-limit spectra) based on the Simplex algorithm. Shin and Freed

Address correspondence to Joseph M. Beechem, Molecular Physiology and Biophysics, 702 Light Hall, Vanderbilt University, Nashville, TN 37232.

0006-3495/93/03/614/08 $2.00

(22) have used the Marquardt-Levenberg algorithm to fit EPR spectra of spin-labels in model membranes to an anisotropic rotational diffusion model.

In the following section a brief review of EPR theory as applied to nitroxide spin-labels is presented. Both rigid-limit and rotational diffusion models are considered. The theory of time-resolved optical anisotropy is also briefly presented. The incorporation of these models into the global analysis fitting procedure is described. In the Results section, we demonstrate the utility of this approach by fitting simulated data and experimental data obtained from the 5-SLE probe.

METHODS

EPR: rigid limit model

In order to fit an EPR spectrum to a dynamic model, accurate values of the rigid-limit A- and g-tensors must first be determined. These can be obtained from a powder pattern fit to a linear EPR spectrum obtained under conditions such that all nitroxide rotational motions have been slowed, as much as possible, to the point where their correlation times are 500 nanoseconds or greater. The orientation dependent spin Hamiltonian for a nitroxide spin-label in a magnetic field is given by

$$\hat{H}(\theta, \phi) = (\beta_e/\hbar)\vec{H}\cdot\mathbf{g}\cdot\vec{S} - \gamma_e\vec{I}\cdot\mathbf{A}\cdot\vec{S}. \quad (1)$$

The electron spin, $\vec{S}$, is coupled to the magnetic field, $\vec{H}$, by the g-tensor and to the nitroxide nitrogen spin, $\vec{I}$, by the A-tensor. These couplings depend on the polar angles θ and ϕ which give the orientation of the (coincident) A- and g-tensors relative to the magnetic field (the lab frame). The total EPR spectrum consists of a sum of Lorentzian lineshapes of finite width, Γ, whose center positions are a function of the nitrogen spin state m_I and the angles θ and ϕ. The appropriate equations are given in detail by Fajer et al. (21). To fully account for various linewidth effects, Γ is taken to be both manifold and orientation dependent.

$$\Gamma(m_I; \theta, \phi) = \Gamma(m_I) + \Gamma_\theta(1 - 3\cos^2\theta) + \Gamma_\phi \sin^2\theta(\cos^2\phi - \sin^2\phi). \quad (2)$$

The simulated powder pattern can be convolved, if necessary, with a Gaussian of width σ to account for inhomogeneous broadening due to weakly coupled protons (or deuterons) not included in the spin Hamiltonian of Eq. 1. The full set of parameters to be found by the nonlinear least-squares powder pattern fit to a spectrum includes the three principal components of the A-tensor, the three principal components of the g-tensor, the $\Gamma(m_I)$, Γ_θ, Γ_ϕ, and σ. The A- and g-tensors thus obtained can be used in fitting linear or ST-EPR data to a rotational diffusion model.

EPR: rotational diffusion model

The spin response of a nitroxide undergoing random motion is given by the quantum mechanical stochastic Liouville equation (9, 23, 24) for the reduced density matrix, $\chi = \sigma - \sigma_{eq}$, where σ_{eq} is the equilibrium density matrix.

$$\dot{\chi} = -i[\hat{H}(\Omega(t)) + \hat{\epsilon}(t), \chi] - \Gamma_R\chi - \Gamma_\Omega\chi - i[\hat{H}(\Omega), \sigma_{eq}], \quad (3)$$

$\hat{\epsilon}(t)$ is the term of the Hamiltonian describing the interaction of the electron spin with the time-dependent microwave field, Γ_R is the phenomenological spin relaxation operator, and Γ_Ω is the operator describing the stochastic motion of the nitroxide. This equation contains a combination of spin variables which are treated quantum mechanically and orientation variables, Ω, which are treated classically. These two sets of variables are coupled through the orientation-dependent spin Hamiltonian. The stochastic fluctuations in $\hat{H}(\Omega(t))$ produce characteristic changes in the EPR spectrum. The simulation program used, developed by Robinson and Dalton (20), solves Eq. 3 for anisotropic Brownian rotational motion and allows for the possibility of calculating ST-EPR spectra including the effects of the time-dependent Zeeman field modulation and saturating microwave power. The rotational diffusion operator is given by:

$$\Gamma_\Omega = -\nabla\cdot\boldsymbol{D}\cdot\nabla. \quad (4)$$

The diffusion tensor, $\boldsymbol{D}$, is diagonal in the molecular frame. For axial rotational diffusion, $\boldsymbol{D}$ has two unique elements.

$$\boldsymbol{D}_d = \begin{bmatrix} D_\parallel & 0 & 0 \\ 0 & D_\parallel & 0 \\ 0 & 0 & D_\perp \end{bmatrix}. \quad (5)$$

The diffusion tensor in the frame of the A- and g-tensors is given by an Euler angle rotation

$$\mathbf{D}(\psi_{tilt}, \theta_{tilt}, \phi_{tilt}) = \mathbf{R}(\psi_{tilt}, \theta_{tilt}, \phi_{tilt})\cdot\boldsymbol{D}_d\cdot\boldsymbol{R}^{-1}(\Psi_{tilt}, \theta_{tilt}, \phi_{tilt}), \quad (6)$$

where the rotation operator, $\boldsymbol{R}$, is defined in Edmonds (25). For isotropic rotational diffusion, there is only one unique element D, the Stokes-Einstein rotational diffusion coefficient, and the rotation in Eq. 6 is irrelevant.

As in the rigid-limit case, the simulated spectra can be convolved with a Gaussian of width σ, if needed, to match the experimental lineshape. The set of parameters varied to fit the data are $D_\parallel$, $D_\perp$, σ, and the relevant tilt angles for axial diffusion, or D and σ for isotropic diffusion.

Time-resolved optical anisotropy

Time-resolved fluorescence and phosphorescence spectroscopies both utilize the following definition of the anisotropy function (26):

$$r(t) = \frac{I_\parallel - GI_\perp}{I_\parallel + 2GI_\perp}, \quad (7)$$

where $I_\parallel$ and $I_\perp$ are, respectively, the measured emission intensities parallel and perpendicular to the vertically polarized excitation and G compensates for the polarization bias of the detection instrumentation. The anisotropy function can be directly related to the rotational diffusion coefficients by

$$r(t) = \sum_i \beta_i e^{(-t/\phi_i)}. \quad (8)$$

The β_i are trigonometric functions of the angles relating the absorption and emmision dipoles to the rotational diffusion tensor and the $1/\phi_i$ are linear combinations of the rotational diffusion coefficients. For the case of axial rotational diffusion,

$$\beta_1 = 0.1(1 - 3\cos^2\theta_a)(1 - 3\cos^2\theta_e)$$
$$\beta_2 = 0.3\sin^2\theta_a\sin^2\theta_e\cos 2\psi_{ae}$$
$$\beta_3 = 1.2\sin\theta_a\cos\theta_a\sin\theta_e\cos\theta_e\cos\psi_{ae}, \quad (9)$$

where θ_a and θ_e are the angles made by the absorption and emission dipoles with respect to the symmetry axis of the diffusion tensor, ψ_{ae} is the angle between the projections of the two dipoles onto the plane perpendicular to the symmetry axis, and

$$\frac{1}{\phi_1} = 6D_\perp \quad \frac{1}{\phi_2} = 4D_\parallel + 2D_\perp \quad \frac{1}{\phi_3} = 5D_\perp + D_\parallel \quad (10)$$

For isotropic rotation diffusion, $r(t)$ decays as a single exponential with ϕ equal to the isotropic rotational correlation time $\tau_r = 1/6D$. The orientation of the absorption and emission dipoles within the molecular frame is irrelevant, but the amplitude of the anisotropy does depend on their relative orientation.

For time-resolved phosphorescence, the anisotropy function is usually fit directly to Eq. 8, as the measured rotational correlation times are much greater than the excitation pulsewidth. In time-resolved fluorescence spectroscopy, one can not directly fit the anisotropy function due to convolution effects and instead one simultaneously fits the observed polarized intensities, $I_\parallel$ and $I_\perp$ (27–29).

Marquardt-Levenberg

The nonlinear least-squares analysis has been performed using the Marquardt-Levenberg algorithm (2, 3, 30). Derivatives of the model functions with respect to the fitting parameters are calculated numerically using the forward difference method in order to minimize the number of EPR lineshape simulations. Fitting for N parameters requires $N + 1$ simulations per iteration.

Because of the fact that simulations of EPR spectra are computationally slow (particularly when dynamic models are used), special attention has been paid to reducing the number of parameters to be fit by the Marquardt-Levenberg algorithm and to increasing the speed of each individual simulation. When fitting to a rigid-limit model, it has been found convenient to form a common linear combination of the elements of the **g**-tensor.

$$\begin{aligned} \bar{g} &= (1/3)(g_{xx} + g_{yy} + g_{zz}) \\ g' &= (1/2)(\bar{g} - g_{zz}) \\ g'' &= (1/2)(g_{xx} - g_{yy}). \end{aligned} \quad (11)$$

The value of $\bar{g}$ can only be determined to the same precision that the microwave frequency, ω_0, and the magnetic field axis are known. The EPR spectrometer used (Bruker ESP-300) only gives ω_0 to three significant figures, while all known values of $\bar{g}$ fall roughly within the range 2.0055–2.0065. Given this small range of possible values and the relatively small anisotropy of nitroxide **g**-tensors, a small change in $\bar{g}$ is essentially equivalent to a change in ω_0. It has proven computationally efficient to choose a fixed $\bar{g}$ and account for any error in this value (or the fixed values of ω_0 and the magnetic field axis) by applying a small post-simulation shift, δH, to the field values of the simulation. The **g**-tensor parameters fit are g' and g'', thus the effective number of fitting parameters is reduced by one. The optimal (minimum χ^2) δH is determined for each simulation by a simple, computationally fast binomial search algorithm. In order to compare the simulation to the data at the same field values, a cubic spline interpolation is used (31). This also allows for the simulation to be calculated at far fewer points than the total number of experimental data points collected. With broad linewidths, a 70–80 Gauss wide spectrum can be efficiently and reliably fit by calculating as few as 200 simulation points. Finally, the minimum χ^2 scale factor and baseline correction to the simulation are obtained by linear least-squares. To summarize the procedure used for any given set of parameters, the EPR powder pattern is calculated, a Gaussian convolution is applied if necessary, and then the optimal value of δH is determined using a simple search routine. For each value of δH tried, a cubic spline interpolation of the simulation is used to match the field values of the simulation to those of the data, then the optimal scale factor and baseline shift are calculated using linear least-squares.

The simulations for the rotational diffusion model are overlaid on the data in the same way, using a small adjustable field axis shift and a scale factor and baseline correction obtained by linear least-squares. Using a cubic spline interpolation to overlay a reduced number of simulation points on a 1024 or 512 point data set is critical to achieving a fit in a reasonable period of time.

Global analysis

The term global analysis refers to the simultaneous analysis of data sets from multiple experiments with an emphasis on fitting directly to a particular physical model. The practical aspects of global analysis have been reviewed elsewhere (2, 3). Both time-resolved optical anisotropy decays and EPR lineshapes have a well-defined dependence on the rotational diffusion coefficients. In addition, it should be noted that the tilt angles in Eq. 6 are directly analogous to the angles θ_a, θ_e, and ψ_{ae} in Eq. 9. The tilt angles define the angular relation between the principal axis frame of the **A**- and **g**-tensors to that of the diffusion tensor, while θ_a, θ_e, and ψ_{ae} define the orientation of the absorption and emission dipoles within the frame of the diffusion tensor. However, in the absence of a known orientational relation between the **A**- and **g**-tensors of the nitroxide and the absorption and emission dipoles of the fluorophores these parameters cannot currently be linked, i.e., related to each other by some mathematical relationship. All of the fits shown in this report were for an isotropic rotational diffusion model. In this case, the orientation parameters are not a factor. However, we note that the method presented here is a potentially powerful tool for fitting data to anisotropic rotational diffusion models.

The uncertainty in the polarization anisotropy data was calculated by assuming Poisson noise for the vertical and horizontal emission intensities and using propagation of errors. The uncertainty in EPR data was estimated from the noise level in the baseline regions of the spectrum assuming uniform noise. These weighting factors are used in the minimization of the global χ^2 defined by

$$\chi^2 = \frac{\sum_{i=1}^{N_{\text{optical}}} \frac{(\text{optical data}_i - \text{optical fit}_i)^2}{\sigma_i^2} + \sum_{j=1}^{N_{\text{EPR}}} \frac{(\text{EPR data}_j - \text{EPR fit}_j)^2}{\sigma_j^2}}{(N_{\text{optical}} + N_{\text{EPR}} - M - 1)}, \quad (12)$$

where N_{optical} and N_{EPR} are the total number of optical and EPR data points respectively, M is the total number of fitting parameters, and the σ_i and σ_j are the estimated uncertainties in the data sets.

All computer programs were written in FORTRAN and run on a Ardent Titan mini-supercomputer running under the Unix operating system. For a given set of parameters, a typical 200 point simulation of a nitroxide powder pattern took ~20 s while the ST-EPR spectrum of a ^{15}N spin-label undergoing isotropic rotational diffusion took approximately 30 min. The time required to generate a simulation varies considerably depending on the nitrogen isotope (^{15}N versus ^{14}N), the rotational model (isotropic versus axial diffusion), and the experiment (linear versus ST-EPR). For the most computationally intensive case considered (the fit to the combined data for 5-SLE/BSA in 86% glycerol, Fig. 7) a complete analysis could be accomplished in 12–16 h.

RESULTS

Fig. 1 shows a powder pattern fit to the linear EPR spectrum of 5-SLE noncovalently bound to bovine serum albumin (BSA) in 86% glycerol at 2°C using the Marquardt-Levenberg algorithm. The linear EPR spectra of 5-SLE noncovalently bound to BSA in 70, 75, 80, and 86% glycerol were all essentially equivalent, demonstrating that the effective rigid limit, on the linear EPR time scale, has been achieved under these conditions. As may be the case in non-linear least-squares analysis, it was found for the rigid-limit model that the final fit depended on the initial starting values chosen for the A-

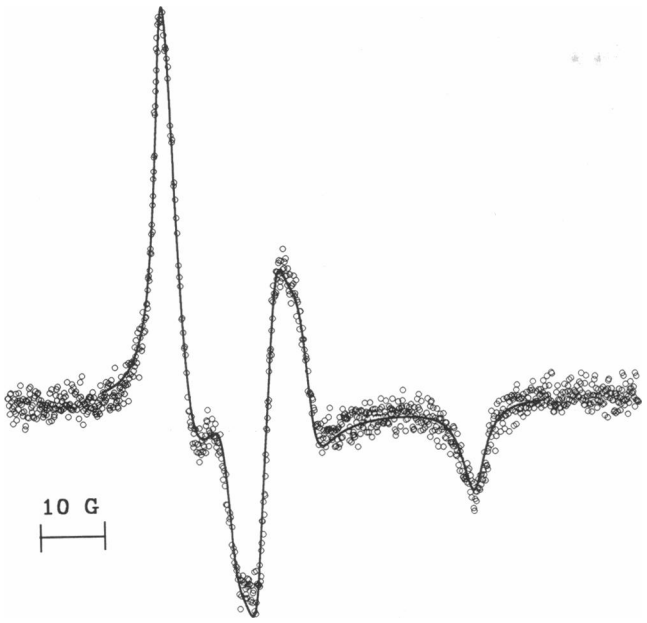

FIGURE 1 Fit to the linear EPR spectrum of 5-SLE/BSA in 86% (wt/wt) glycerol at 2°C. The sample was described in the preceeding article (1). The best-fit parameters obtained were g_{xx} = 2.008431, g_{yy} = 2.005956, g_{zz} = 2.002114, A_{xx} = 8.057 Gauss, A_{yy} = 8.620 Gauss, A_{zz} = 47.768 Gauss, $\Gamma(-1/2) = \Gamma(+1/2)$ = 2.051 Gauss, Γ_θ = −0.091 Gauss. The values of Γ_ϕ and σ were fixed to zero. The value of $\bar{g}$ was fixed to 2.005500. The spectral width displayed is 100 Gauss.

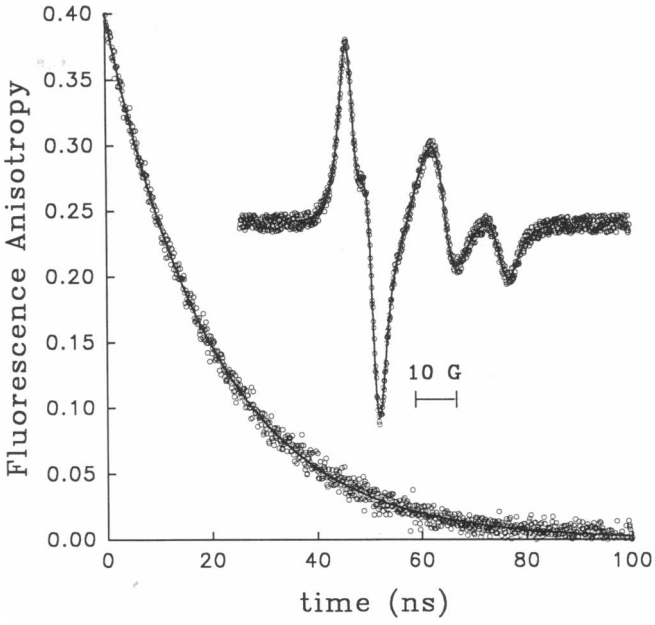

FIGURE 2 Simultaneous fits to simulated time-resolved fluorescence and linear EPR (*upper right*) data. The simulated data were generated using an isotropic rotational correlation time of 20.00 nanoseconds. The value recovered from the global analysis is τ_r = 20.06 nanoseconds.

and g-tensors. However, the overall computational speed and efficiency of the method described here allowed for a number of initial parameter sets to be tried and a true minimum χ^2 to be found. It should be noted that a small orientation dependent linewidth, Γ_θ, proved critical to obtaining accurate tensor values. Without an anisotropic linewidth, the high field z-turning point could not be fit properly. The A- and g-tensors obtained from this fit are used below to fit the ST-EPR data.

Fig. 2 shows the simultaneous fits to simulated fluorescence anisotropy and linear EPR data. The simulated data were generated assuming an isotropic rotational correlation time ($\tau_r = 1/6D$, $D = D_\parallel = D_\perp$) of 20 nanoseconds. Poisson noise was added to the optical data (18,000 peak counts in $I_\parallel$) and uniform noise added to the EPR data. The value recovered from the global analysis was τ_r = 20.06 nanoseconds. Fig. 3 shows the χ^2 surface for the simultaneous fit to the combined data sets compared to the χ^2 surface for the fit to the EPR data alone. It is clear that, in this idealized case, the uncertainty in τ_r obtained from the fit to the EPR data decreased when the global analysis of the combined EPR and optical data sets is performed.

Fig. 4 shows the simultaneous fit to the time-resolved phosphorescence anisotropy and ST-EPR data from 5-SLE/BSA at 2°C in 70% (wt/wt) glycerol. The ST-EPR spectrum was fit to an isotropic rotational diffusion model varying τ_r and σ. The phosphorescence anisotropy decay was fit to the sum of two exponentials, the longer of the two time constants is taken to be the isotropic rotational correlation time (1). The values of τ_r used to fit the two data sets were linked (required to be equal).

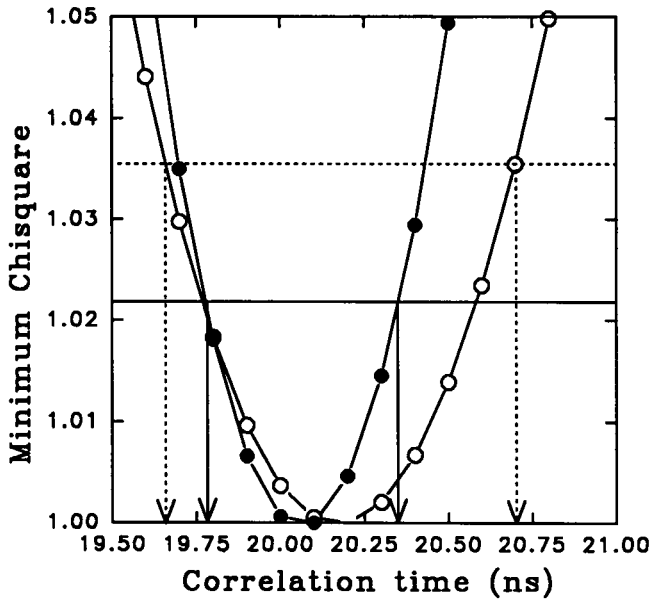

FIGURE 3 Comparison of the χ^2 error surfaces as a function of τ_r for the simultaneous fit (*solid circles*) and the fit to the EPR data alone (*open circles*). The arrows show the 66.6% confidence interval (as estimated using the F-statistic) for the values of τ_r obtained from the two fits.

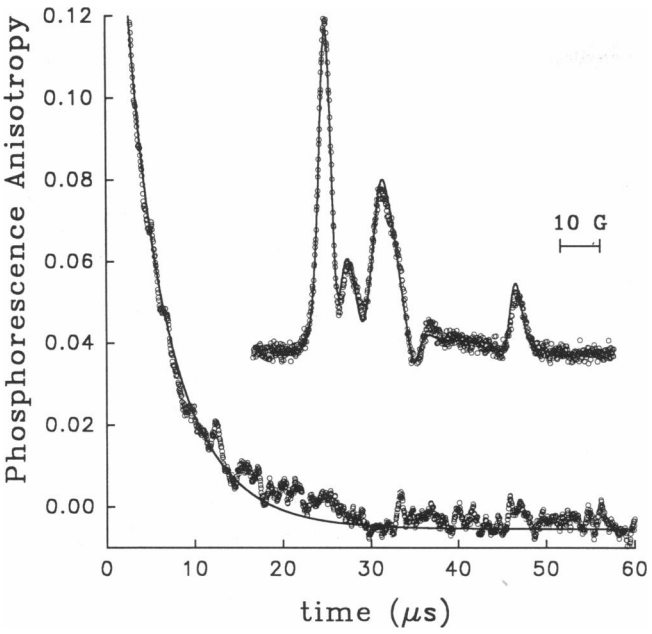

FIGURE 4 Simultaneous fit to the phosphorescence anisotropy and ST-EPR (*upper right*) data from 5-SLE/BSA at 2°C in 70% (wt/wt) glycerol. The data is taken from Figs. 5 and 7 of the preceeding article (1). The value of τ_r obtained from the global analysis is 5.62 μsec (σ = 1.40 Gauss). Additional (fixed) input parameters were as follows: **A**- and **g**-tensors from the fit to the linear EPR spectrum in Fig. 1; T_{1e} = 27. × 10^{-6} s; T_{2e} = 40. × 10^{-9} seconds; microwave power h_1 = 0.180 Gauss.

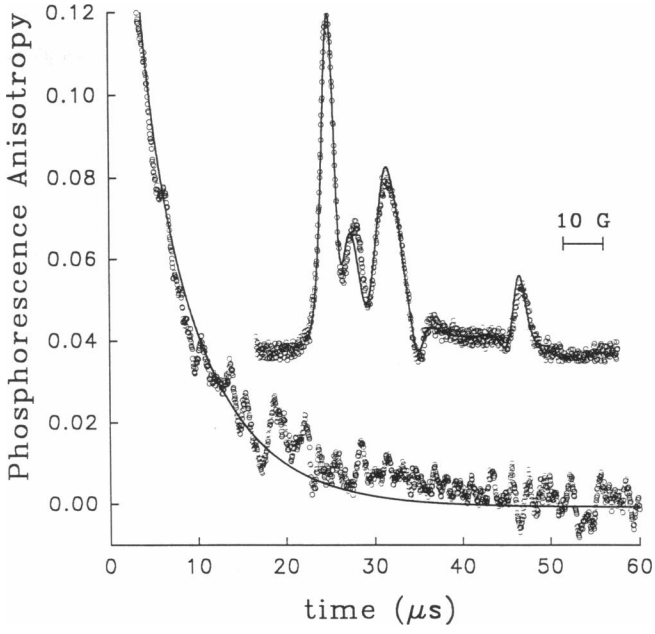

FIGURE 5 Same as Fig. 4 for the 75% (wt/wt) glycerol data. The value of τ_r obtained from the global analysis is 7.15 μs (σ = 1.41 Gauss). All other parameters were as in Fig. 4.

Typically, convergence was obtained after 3 to 10 iterations and the final result did not depend significantly on the initial parameter set. Figs. 5, 6, and 7 shows the simultaneous fits to the time-resolved phosphorescence anisotropy decay and ST-EPR data for 5-SLE/BSA in 75, 80, and 86% glycerol, respectively.

The values of τ_r obtained from the simultaneous analyses of the ST-EPR and phosphorescence anisotropy data are plotted versus the viscosity divided by absolute temperature (η/T) in Fig. 8. According to the Stokes-Einstein equation,

$$\tau_r = \frac{4\pi\eta r_h^3}{3kT},$$

the slope of this line is proportional to the cube of the hydrodynamic radius, r_h, of the 5-SLE/BSA complex. The value of r_h obtained from this plot is 31.8 Å, which agrees well with the values obtained from independent analysis of the phosphorescence anisotropy or ST-EPR data (1).

DISCUSSION

The natural extension of combining both a fluorophore and a nitroxide radical within the same probe molecule is to combine both optical and EPR data into a single analysis. The principle reasons for performing a global analysis of the optical and EPR data are (*a*) to rigorously test particular rotational models, (*b*) to use the increased information content of the combined data sets, and (*c*) to increase the resolution of the fitting parameters. The results presented by Cobb et al. (1) demonstrate that both time-resolved optical anisotropy and EPR are mon-

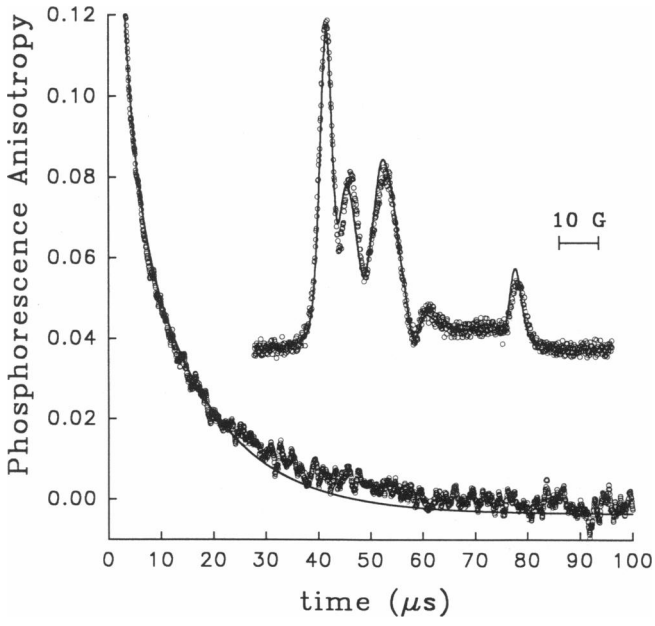

FIGURE 6 Same as Fig. 4 for the 80% (wt/wt) glycerol data. The value of τ_r obtained from the global analysis is 13.93 μs (σ = 1.32 Gauss). All other parameters were as in Fig. 4, except h_1 = 0.200 Gauss.

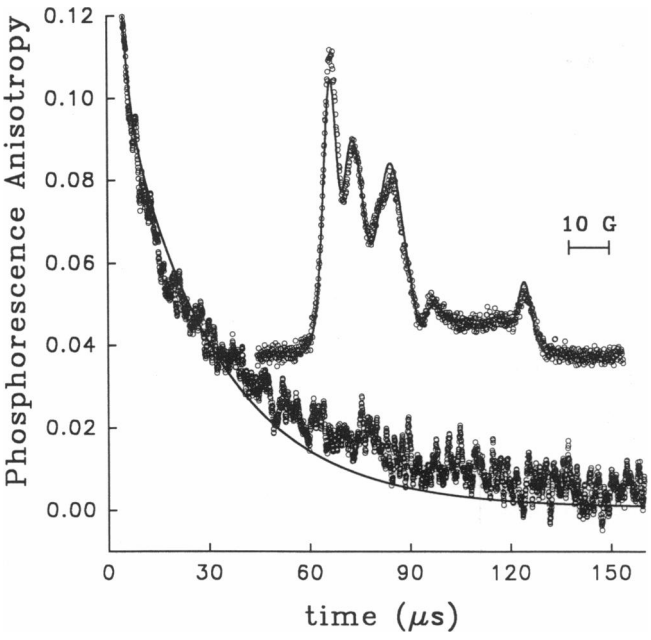

FIGURE 7 Same as Fig. 4 for the data 86% (wt/wt) glycerol data. The value of τ_r obtained from the global analysis is 27.95 μs (σ = 1.44 Gauss). All other parameters were as in Fig. 4, except h_1 = 0.225 Gauss.

itoring the same large scale Brownian motions (although local motion may be different). The combined analysis of the EPR and optical data presented here clearly show that data from both optical and EPR experiments can be simultaneously fit to a single model.

The two experimental techniques considered are fundamentally different. Fluorescence anisotropy and linear EPR are sensitive to motions on the same time scales, as are phosphorescence anisotropy and ST-EPR, but these sensitivities are governed by different properties. In the optical emission spectroscopies, one is limited to the determination of rotational correlations times which are on the order of the total intensity lifetime of the probe (or less). The motional sensitivity of linear EPR is governed by the anisotropy of the **A**- and **g**-tensors and that of ST-EPR by T_{1e}. In the time-resolved optical anisotropy experiment, a select distribution of molecular orientations is excited by the vertically polarized excitation pulse. The decay of this distribution back to equilibrium is monitored by $r(t)$ which can be fit directly to a set of correlation times. In EPR, the orientation dependent resonance position of an electron spin is modulated by stochastic motion. The effect of this motion on the EPR spectrum can only be determined by solution of Eq. 3. There is no direct way to extract correlation times from the data.

The two techniques have different sensitivities to anisotropic rotational diffusion. Time-resolved optical anisotropy is governed by the orientation of the absorption and emission dipoles in the frame of the diffusion tensor. Unfortunate combinations of the angles in Eq. 9 can result in a loss of sensitivity to one component of the motion. On the other hand, EPR is governed by the three-dimensional **A**- and **g**-tensors. There is no orientation of these tensors relative to the diffusion tensor for which the EPR spectrum will not be at least somewhat sensitive to all components of the rotational diffusion tensor (15). The **g**-tensor is more non-axial in character than the **A**-tensor and its influence scales linearly with the magnetic field. Performing EPR experiments at two or more frequencies (e.g., X and Q band) allows one to vary the sensitivity to motion about the nitroxide z-axis versus motion about the x- and y-axes in a well defined way (32). The analysis of such data would obviously benefit from the global analysis approach.

As was seen in the case of 5-SLE noncovalently bound to BSA, the presence of multiple components, with different rotational properties, can complicate the data analysis (1). In an optical experiment, a multiple component system will give a multi-exponential anisotropy decay curve. There can, however, be an ambiguity as to whether this is due to multiple components or a single component undergoing anisotropic rotational diffusion. Furthermore the amplitudes, β_i (Eq. 9), of the exponential decays depend not only on concentration but also the orientation of the dipoles to the diffusion tensor. In EPR, the spectra of the two species will overlap, but if the correlation times are sufficiently different the spectra can be separated and the concentration of each species determined directly from the integrated intensities of the two spectra. Because of the Zeeman modulation detec-

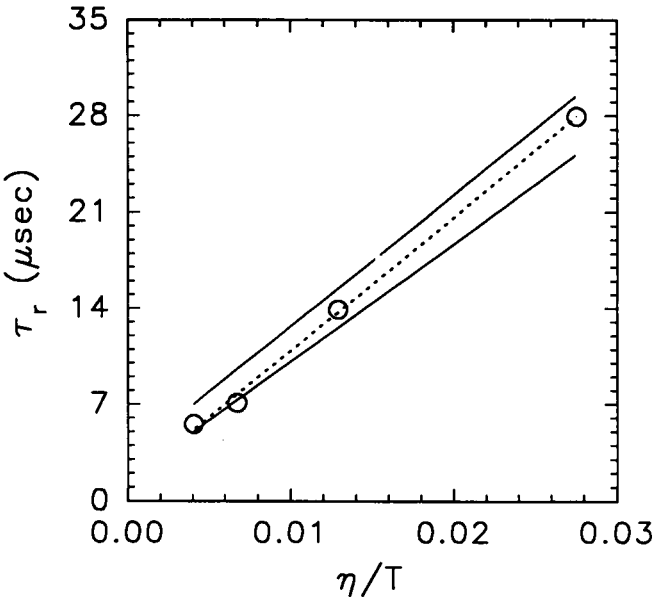

FIGURE 8 Plot of the four values of τ_r (*circles*) determined in Figs. 4 through 7 versus η/T. From the slope of the linear least-squares fit (*dashed line*) to these values, r_h was determined to be 31.8 Å. The solid lines are the linear fits to the values of τ_r obtained by independent analysis of the phosphorescence anisotropy and EPR data (1).

tion scheme used, EPR has a particularly high sensitivity to small populations of molecules undergoing fast ($\tau_r < 10^{-9}$ seconds) motion.

In the preceeding paragraphs, we mention several examples of the complementary nature of time-resolved optical anisotropy and EPR. The interested reader is directed to recent reviews by Thomas who has discussed these points in more detail (14, 15). The differences between the two techniques become an advantage when global analysis is used. If a single physical model is found to fit data from both techniques, there is a high probability that the model is correct.

In the current analyses of optical and EPR data only the rotational diffusion coefficients are linked. However, the global analysis program has been designed to allow linkage of the angular dependent terms also. This could be achieved if the relative orientations of the **A**- and **g**-tensors of the nitroxide and the absorption and emission dipoles of the fluorophores were known. Small molecule x-ray crystallography, molecular modeling, or studies using oriented samples may be able to provide this information. Burghardt and co-workers (16, 17) have reported an interesting example of how the relative orientations of different probes can be determined. In addition, data obtained at multiple temperatures, viscosities, excitation/emission wavelengths (optical), or microwave frequencies (EPR) may be combined together within a single global analysis.

It is important to emphasize that the present work has provided a definition of a flexible computational framework for the global nonlinear analysis of combined time-resolved optical anisotropy and EPR data and for the determination of rotational diffusion properties of biomolecules. The model system considered, 5-SLE/BSA, provided an opportunity to test this approach. Clearly, for this simple system, analysis of the EPR or optical data alone provided a reasonable description of the global rotational dynamics as demonstrated in the preceeding companion article (1). In the combined global analyses shown in Figs. 4–7, the fits to the phosphorescence decays systematically deviate from the data at long times. These deviations suggest that the isotropic model may not be completely adequate to describe the system. However, the goal of this study was not to rigorously characterize the rotational properties of BSA, but simply to show the utility of this methodology.

There are many examples in both the optical and EPR literature where capabilities for more in-depth analysis could be of use in elucidating the dynamic properties of more complicated systems. Detailed information regarding anisotropic rotational diffusion or questions of local versus global dynamics, which can impact directly on important conclusions regarding function, is often difficult to obtain by one technique alone. It is our belief, based on the data and discussion presented, that the acquisition of both optical anisotropy and EPR data (either with dual probes such as 5-SLE or with separate optical and EPR probes), together with the global analysis of these data, can significantly increase the quantity and quality of information obtainable from such studies.

This work was supported in part by grants from the National Institutes of Health HL34737, CA43720, and RR04075 to A.H.B. and GM45990 and RR05823 to J. Beechem J.M.B. is also supported as a Lucille P. Markey Scholar. E. Hustedt was supported by NIH training grant T32 DK07186.

Received for publication 2 September and in final form 10 November 1992.

REFERENCES

1. Cobb, C. E., E. J. Hustedt, J. M. Beechem, and A. H. Beth. 1992. Protein rotational dynamics investigated with a dual EPR/optical molecular probe: spin-labeled eosin. *Biophys. J.* 64:605–613.
2. Beechem, J. M., E. Gratton, M. Ameloot, J. R. Knutson, and L. Brand. 1991. The global analysis of fluorescence intensity and anisotropy decay data: second generation theory and programs. *In* Topics in Fluorescence Spectroscopy, Volume 2: Principles. J. R. Lakowicz, editor. Plenum Press, New York. 241–305.
3. Beechem, J. M. 1992. Global analysis of biochemical and biophysical data. *Methods Enzymol.* 210:37–54.
4. Steiner, R. R. 1991. Fluorescence anisotropy: theory and applications. *In* Topics in Fluorescence Spectroscopy, Volume 2: Principles. J. R. Lakowicz, editor. Plenum Press, New York. 1–51.
5. Cherry, R. J., A. Cogoli, M. Oppliger, G. Schneider, and G. Semenza. 1976. A spectroscopic technique for measuring slow rotational diffusion of macromolecules. 1. Preparation and properties of a triplet probe. *Biochemistry.* 17:3653–3656.
6. Corin, A. F., E. Blatt, and T. M. Jovin. 1987. Triplet-state detection of labeled proteins using fluorescence recovery spectroscopy. *Biochemistry.* 26:2207–2217.
7. Berliner, L. J., editor. 1976. Spin Labeling Theory and Applications. Academic Press, New York. 592pp.
8. Berliner, L. J., editor. 1979. Spin Labeling II Theory and Applications. Academic Press, New York. 357pp.
9. Dalton, L. R., editor. 1985. EPR and Advanced EPR Studies of Biological Systems. CRC Press, Boca Raton, FL. 314pp.
10. Berliner, L. J., and J. Reuben, editors. 1989. Biological Magnetic Resonance, Volume 8, Spin Labeling Theory and Applications. Plenum Press, New York. 650pp.
11. McCalley, R. C., E. J. Shimshick, and H. M. McConnell. 1972. The effect of slow rotational motion on paramagnetic resonance spectra. *Chem. Phys. Lett.* 13:115–119.
12. Thomas, D. D., L. R. Dalton, and J. S. Hyde. 1976. Rotational diffusion studied by passage saturation transfer electron paramagnetic resonance. *J. Chem. Phys.* 65:3006–3024.
13. Thomas, D. D. and H. M. McConnel. 1974. Calculation of paramagnetic resonance spectra sensitive to very slow rotational motion. *Chem. Phys. Lett.* 25:470–475.
14. Thomas, D. D., T. M. Eads, V. A. Barnett, K. M. Lindahl, D. A. Momont, and T. C. Squier. 1985. Saturation transfer EPR and triplet anisotropy: complementary techniques for the study of microsecond rotational dynamics. *In* Spectroscopy and the Dynamics of Molecular Biological Systems. P. Bayley and R. Dale, editors. Academic Press, New York. 239–257.

15. Thomas, D. D. 1986. Rotational diffusion of membrane proteins. *In* Techniques for the Analysis of Membrane Proteins. C. I. Ragan and R. J. Cherry, editors. Chapman and Hall, London. 377–431.
16. Burghardt, T. P., and K. Ajtai. 1992. Mapping global angular transitions of proteins in assemblies using multiple extrinsic reporter groups. *Biochemistry.* 31:200–206.
17. Ajtai, K., A. Ringler, and T. P. Burghardt. 1992. Probing cross-bridge angular transitions using multiple extrinsic reporter groups. *Biochemistry.* 31:207–217.
18. Brand, L., and M. Johnson, editors. 1992. Methods in Enzymology, Volume 210, Numerical Computer Methods. Academic Press, New York. 718pp.
19. Schneider, D. J., and J. H. Freed. 1989. Calculating slow motional magnetic resonance spectra: a user's guide. *In* Biological Magnetic Resonance, Volume 8, Spin Labeling Theory and Applications. Berliner, L. J. and J. Reuben, editors. Plenum Press, New York. 1–76.
20. Robinson, B. H., and L. R. Dalton. 1980. Anisotropic rotational diffusion studied by passage saturation transfer electron paramagnetic resonance. *J. Chem. Phys.* 72:1312–1324.
21. Fajer, P. G., R. L. H. Bennet, C. F. Polnazek, E. A. Fajer, and D. D. Thomas. 1990. General method for multiparameter fitting of high-resolution EPR spectra using a simplex algorithm. *J. Magn. Reson.* 88:111–125.
22. Shin, Y.-K., and J. H. Freed. 1989. Dynamic imaging of lateral diffusion by electron spin resonance and study of rotational dynamics in model membranes. *Biophys. J.* 55:537–550.
23. Freed, J. H. 1976. Theory of slow tumbling ESR spectra for nitroxides. *In* Spin Labeling Theory and Applications. L. J. Berliner, editor. Academic Press, New York. 53–132.
24. Dalton, L. R., B. H. Robinson, L. A. Dalton, and P. Coffey. 1976. in Advances in Magnetic Resonance, Volume 8. J. S. Waugh, editor. Academic Press, New York. 149–259.
25. Edmonds, A. R. 1957. Angular Momentum in Quantum Mechanics. Princeton University Press, Princeton, NJ. 146pp.
26. Jablonski, A. 1960. On the notion of emission anisotropy. *Bull. Acad. Pol. Sci.* 8:259–264.
27. Gilbert, C. W. 1980. A vector model for non-linear least squares reconvolution and fitting analysis of polarized fluorescence decay data. *In* Time-Resolved Fluorescence Spectroscopy in Biochemistry and Biology. R. Cundall and R. Dale, editors. NATO ASI Publication, Plenum Press, New York. 605–606.
28. Cross, A., and G. R. Fleming. 1984. Analysis of time-resolved fluorescence anisotropy decays. *Biophys. J.* 46:45–56.
29. Beechem, J. M., and L. Brand. 1986. Global analysis of fluorescence decay: applications to some unusual and theoretical studies. *Photochem. Photobiol.* 44:323–329.
30. Bevington, P. R. 1969. Data Reduction and Error Analysis for the Physical Sciences. McGraw-Hill, New York. 336pp.
31. Press, W. H., B. P. Flannery, S. A. Teukolsky, and W. T. Vetterling. 1986. Numerical Recipes The Art of Scientific Computing. Cambridge University Press, Cambridge. 818pp.
32. Beth, A. H., and B. H. Robinson. 1989. Nitrogen-15 and deuterium substituted spin labels for studies of very slow rotational motion. *In* Biological Magnetic Resonance, Volume 8, Spin Labeling Theory and Applications. L. J. Berliner and J. Reuben, editors. Plenum Press, New York. 179–249.